Changes in the Profile Structure of the Sarcoplasmic Reticulum Membrane Induced by Phosphorylation of the Ca^{2+}ATPase Enzyme in the Presence of Terbium: A Time-Resolved X-ray Diffraction Study

Francisco J. Asturias, Robert F. Fischetti,* and J. Kent Blasie
Department of Chemistry, University of Pennsylvania, and *Biostructures Institute, University City Science Center, Philadelphia, Pennsylvania 19104 USA

ABSTRACT The design of the time-resolved x-ray diffraction experiments reported in this and an accompanying paper was based on direct measurements of enzyme phosphorylation using [γ-^{32}P]ATP that were employed to determine the extent to which the lanthanides La^{3+} and Tb^{3+} activate phosphorylation of the Ca^{2+}ATPase and their effect on the kinetics of phosphoenzyme formation and decay. We found that, under the conditions of our experiments, the two lanthanides are capable of activating phosphorylation of the ATPase, resulting in substantial levels of phosphoenzyme formation *and* they slow the formation and dramatically extend the lifetime of the phosphorylated enzyme conformation, as compared with calcium activation. The results from the time-resolved, *nonresonance* x-ray diffraction work reported in this paper are consistent with the enzyme phosphorylation experiments; they indicate that the changes in the profile structure of the SR membrane induced by terbium-activated phosphorylation of the ATPase enzyme are persistent over the much longer lifetime of the phosphorylated enzyme and are qualitatively similar to the changes induced by calcium-activated phosphorylation, but smaller in magnitude. These results made possible the time-resolved, *resonance* x-ray diffraction studies reported in an accompanying paper utilizing the resonance x-ray scattering from terbium, replacing calcium, to determine not only the location of high-affinity metal-binding sites in the SR membrane profile, but also the redistribution of metal density among those sites upon phosphorylation of the Ca^{2+}ATPase protein, as facilitated by the greatly extended lifetime of the phosphoenzyme.

INTRODUCTION

The relaxation phase of the contraction-relaxation cycle in striated and cardiac muscle is caused by the active (energy-dependent) transport of Ca^{2+} across the sarcoplasmic reticulum (SR) membrane from the cytoplasm to the sarcotubular system. The enzyme responsible for this process is Ca^{2+}ATPase, which uses chemical energy obtained from the hydrolysis of ATP to move Ca^{2+} ions across the membrane against a maximal concentration gradient of 10^3 M (Inesi, 1985). The SR membrane can be readily isolated and purified in the form of unilamellar vesicles, which contain almost exclusively phospholipids and the Ca^{2+}ATPase protein (>90% of the total protein weight) (MacLennan, 1970; MacFarland and Inesi, 1971; Meisner et al., 1973), and the biochemistry and kinetics of the different steps in the Ca^{2+} transport cycle are well characterized (Inesi, 1985). Consequently, the SR system is an excellent model for the study of active ion transport across membranes. X-ray and neutron diffraction studies have provided information about the separate, low-resolution profile structures of the Ca^{2+}ATPase and the phospholipid bilayer within the isolated membrane (Herbette et al., 1985), and electron crystallographic studies of two-dimensionally crystalline forms of the ATPase have provided some low-resolution information about the three-dimensional structure of the protein (Stokes and Green, 1990). However, the lack of high-resolution three-dimensional structural information for the Ca^{2+}ATPase has made it difficult to elucidate the mechanism of Ca^{2+} active transport by the enzyme.

Time-resolved x-ray diffraction studies (Blasie et al., 1985; Pascolini et al., 1988), as well as results from other experimental techniques (DuPont, 1980; DuPont et al., 1988), have revealed the existence of conformational changes in the Ca^{2+}ATPase upon phosphorylation of the protein ($M_xE \rightarrow M_xE{\sim}P$).[1] The results from the time-resolved x-ray diffraction studies show that specific, large-scale conformational changes occur across the entire membrane profile and indicate that the observed changes are essential for the Ca^{2+} active transport function of the protein (Blasie et al., 1990). Determination of the locations of metal-binding sites in the membrane profile for the different conformations of the Ca^{2+}ATPase would be especially relevant for the elucidation of the Ca^{2+} transport mechanism. We have reported the existence and location of discrete, high-affinity metal-binding/transport sites in the membrane profile for the resting unphosphorylated conformation of the Ca^{2+}ATPase, identified via lanthanide resonance x-ray diffraction studies (Asturias and Blasie, 1991). Our results concerning the location of these metal-binding/transport sites are in general agreement with the predicted locations for such sites based

Received for publication 29 January 1993 and in final form 16 February 1994.

Address reprint requests to J. Kent Blasie, Department of Chemistry, Chemistry Building, University of Pennsylvania, Philadelphia, PA 19104-6323. Tel.: 215-898-6208; Fax: 215-898-6242.

0006-3495/94/05/1653/12 $2.00

[1] The notation M_xE is used to indicate which metal is occupying the binding/transport sites of the Ca^{2+}ATPase and activating the enzyme for phosphorylation. $M_xE{\sim}P$ represents the phosphorylated enzyme conformation. We have purposely chosen not to indicate a particular binding stoichiometry.

on results obtained from other less direct experimental techniques (Clarke et al., 1989). After binding of Ca^{2+} to the unphosphorylated conformation of the ATPase, phosphorylation is the first necessary step in the cycle of reactions that occurs during Ca^{2+} transport. Therefore, extension of the resonance diffraction work to this next step in the Ca^{2+} transport cycle (protein phosphorylation) would provide information on how the changes observed in the profile structure of the Ca^{2+}ATPase upon enzyme phosphorylation affect the location in the membrane profile of the previously identified metal-binding/transport sites, and the distribution of metal-atom density among them. The presence of a metal ion (generally Ca^{2+}) at the high-affinity binding/transport sites on the ATPase is an essential requirement for activation of the enzyme for phosphorylation (Makinose, 1969). Therefore, before the lanthanide resonance x-ray diffraction work can be extended to include the phosphorylated enzyme conformation, it is necessary to determine whether lanthanides can act as the activating metal ion for phosphorylation of the Ca^{2+}ATPase, and if so, to determine the properties of the phosphorylated enzyme intermediate formed in the presence of lanthanides. The results reported in this paper show that lanthanides are indeed capable of replacing Ca^{2+} as the metal ion responsible for activation of the ATPase for phosphorylation, and that large-scale changes in the profile structure of the SR membrane observed upon lanthanide-activated phosphorylation of the ATPase are qualitatively similar in nature to the changes that occur upon calcium-activated phosphorylation of the protein. These findings substantiate the physiological significance of the results obtained from our structural studies of the Ca^{2+}ATPase using lanthanides as Ca^{2+} analogs, and have also established the necessary basis for further time-resolved, resonance x-ray diffraction work that has provided information about the locations and changes in occupancy of metal-binding/transport sites in the profile structure of the Ca^{2+}ATPase enzyme upon its phosphorylation.

MATERIALS AND METHODS

Preparation of SR vesicular dispersions and oriented SR multilayers. Measurement of enzyme phosphorylation and phosphoenzyme lifetime in the presence of Ca^{2+}, La^{3+}, or Tb^{3+}

Dispersions of SR membrane vesicles were prepared from albino rabbit hind leg muscle (MacFarland and Inesi, 1971). This SR preparation will be referred to as "crude SR," and its protein content of ~10–15 mg/ml (determined according to Lowry et al., 1951) is typically approximately 67% Ca^{2+}ATPase; it is comparable to those normally utilized for kinetic studies reported in the literature (Inesi et al., 1988; Squier et al., 1990), and it was used for most of our enzyme phosphorylation studies. Primarily for the x-ray diffraction experiments, the SR preparation was further purified by sucrose density gradient centrifugation, as described previously (Meisner et al., 1973). This purified SR preparation will be referred to as "pure SR," and its protein content (determined according to Lowry et al., 1951) is also ~10–15 mg/ml and is typically over 90% Ca^{2+}ATPase. The crude SR preparations were suspended in 30% sucrose containing 10 mM histidine at pH 7.0 and stored at −70°C until used. The pure SR preparations were usually (see below) suspended in a buffer containing 120 mM KCl, 10 mM $MgCl_2$, 40 mM Tris maleate (pH 6.85), and stored at −70°C until used.

Mostly crude SR preparations were utilized for the measurements of enzyme phosphorylation and phosphoenzyme lifetime in the presence of calcium, lanthanum, or terbium. However, to ensure that the enzyme phosphorylation experiments were not dependent on the SR preparation utilized, a number of measurements were also performed with the pure SR preparation used for the x-ray diffraction experiments. In this case, the only difference was that no $MgCl_2$ was added to the final storage buffer so that the divalent metal cation concentration could be varied as necessary for the phosphorylation experiments.

The extent of phosphoenzyme formation from [γ-^{32}P] ATP in the presence of calcium, lanthanum, or terbium was measured using a procedure described in the literature (Inesi et al., 1988). For the assays, the SR vesicular preparations were suspended (final protein concentration ~0.5–0.6 mg protein/ml) in a buffer containing 80–100 mM KCl, 20 mM MOPS (3-[*N*-morpholino]propanesulfonic acid), and the desired (see Results) Mg^{2+} concentration. In some cases, to control even further the divalent metal conditions under which enzyme phosphorylation was measured, the SR vesicles were treated with EGTA ([ethylene-(oxyethylenenitrilo)]tetraacetic acid) and subsequently washed with multivalent metal cation-free buffer (treated with Chelex-100 (Bio-Rad Laboratories, Richmond, CA)) via dilution and centrifugation. The desired (see Results) concentration of the activating metal cation (Ca^{2+}, La^{3+} or Tb^{3+}) was then added and the enzyme incubated with the activating cation for a period of time, varying from 5 to 600 s. After incubation with the activating metal cation, the desired (see Results) concentration of labeled ATP was added to the reaction mixture; the reaction was allowed to proceed at the desired temperature (~4°C) and was subsequently "quenched" by the addition of 1 M $HClO_4$/4 mM H_3PO_4. The "quenched" protein samples were centrifuged, and the level of phosphoenzyme formation was determined. The final results (expressed as nmol of phosphorylated protein/mg ATPase) were then plotted as a function of the time elapsed from the moment when the phosphorylation reaction was initiated (addition of [γ-^{32}P]ATP)) until it was acid-quenched.

To prepare oriented multilayer samples for the x-ray diffraction studies, an appropriate volume of the pure SR dispersion (enough to obtain ~1.2 mg of protein) was placed in a sedimentation cell containing 500 μl of the same buffer solution in which the purified SR vesicles were stored. A small volume of a freshly prepared $TbCl_3$ solution was added to obtain the desired 4:1 Tb^{3+}/protein molar ratio (Tb^{3+} was used for the x-ray diffraction experiments because of the higher energy location of its L_{III} absorption edge, and also because of its higher capacity to displace Ca^{2+} from the high-affinity binding/transport sites on the ATPase protein; see Discussion). Finally, glutathione and caged ATP (final concentration ~5 mM; CalBiochem, San Diego, CA) were added to the cell, whose contents were then carefully mixed. The above operations were carried out in a cold room and under dim light to preserve the functionality of the samples and prevent any photolysis of the caged ATP. The contents of the sedimentation cell were then centrifuged ($10^4 \times g$ for 45 min) to sediment the SR vesicles onto a flat aluminum foil substrate, and the resulting "pellet" was partially dehydrated in a sealed glass vial over a saturated KCl solution (88% relative humidity at ~4°C) to form an oriented SR membrane multilayer sample, as described previously (Herbette et al., 1977). The Ca^{2+}ATPase concentration in the equilibrated, partially dehydrated multilayer specimens was ~5 mM, and the concentrations of Tb^{3+} and caged ATP were ~20 mM (4:1 Tb^{3+}/ATPase mole ratio) and ~10 mM (2:1 caged ATP/ATPase mole ratio), respectively.

X-ray data collection

For the x-ray diffraction experiments, the SR multilayer samples (formed through controlled partial dehydration of the wet SR pellets prepared by centrifugation) were quickly transferred to a temperature-controlled, sealed specimen chamber. The temperature in the specimen chamber was kept constant at 4°C, and the relative humidity was carefully controlled with a home-built "humidity controller," designed after specifications published in the literature (Gruner, 1981). The humidity controller circulated a small flow of moist helium through the specimen chamber and made it possible to keep a constant relative humidity of 85 ± 1% during the x-ray experiment. A small opening (covered with thin Mylar film) allowed the UV light used to

photolyze the caged ATP to reach the sample. The photolysis light (300–370 nm) was provided by a 200 W mercury-arc lamp and delivered to the sample via a liquid light guide (Oriel Optics, Stratford, CT).

Lamellar X-ray diffraction data from the oriented, partially dehydrated SR multilayers was collected as a function of the reciprocal space coordinate z^* ($z^* = 2 \sin \theta/\lambda$). Diffraction along this z^* axis corresponds to elastic photon momentum transfer parallel to the real space axis z, defined as perpendicular to the plane (on average) of the membranes of the flattened vesicles in the oriented multilayer sample. Diffracted intensity along z^* arises from the so-called multilayer electron density profile, that is, from the projection onto the z-axis of the multilayer electron density along planes perpendicular to the z-axis (Blasie et al., 1985).

The lamellar x-ray diffraction data were collected utilizing the Biostructures Participating Research Team beamline X-9A at the National Synchrotron Light Source, Brookhaven National Laboratory (Upton, NY). During data collection, the synchrotron operated at an electron energy of 2.5 GeV, and the current in the ring decayed during a fill from 200 to 90 mA. A focusing, constant-exit-height, double Si(111) crystal monochromator was used to select the energy of the x-ray radiation incident on the samples and to provide partial focusing of the monochromatic x-ray beam in the horizontal direction (perpendicular to z^*). The monochromator energy was calibrated by recording the x-ray absorption spectrum from a powdered $TbCl_3 \cdot 6H_2O$ sample, and was further confirmed by determining the position of the terbium L_{III} absorption edge recorded directly from a SR multilayer sample containing the lanthanide.

Radiation from the monochromator (FWHM 2.5 eV) was collected and focused in the vertical direction (parallel to z^*) at the detector using a cylindrically bent horizontal mirror (Ni-coated Al), with its center at 1340 cm from the bending-magnet source. The cylindrically curved multilayer samples were mounted on a 4-circle diffractometer (Huber, FRG), with their surface centered on, and parallel to, the ω-axis. The beamline optics and associated electronics were controlled by a PDP 11/23 computer (Digital Equipment Corp., Marlboro, MA). Lamellar diffraction patterns were recorded with a two-dimensional, position-sensitive proportional counter (Siemens Analytical X-ray Instruments, Inc., Madison, WI), mounted on the 2θ-axis, 680 mm from the ω-axis. The detector was interfaced to a dedicated GPXII MicroVAX computer (Digital) that was used to store the two-dimensional diffraction patterns and also to control the 4-circle diffractometer. The cross section of the doubly-convergent x-ray beam was further defined using both defining- and guard-slits, and the final beam had a FWHM at the sample of ~0.4 mm parallel to z^*, and of ~1.5 mm in the perpendicular direction. An N_2-filled ionization chamber was used to monitor the incident beam intensity, I_0.

Once the SR multilayer sample had been mounted in the specimen chamber, it was allowed to stabilize for 30–60 min. During this time, short (60–300 s) diffraction patterns were collected at a single x-ray energy (corresponding to the terbium L_{III} absorption edge) to monitor the time evolution and stability of the sample. Subsequent patterns were compared to monitor the stabilization of the sample, and when arithmetic differences between consecutive patterns were equal to zero (to within the counting statistics noise), the sample was considered stable, and the actual experiment was started. Lamellar diffraction patterns were collected at three different energies: the terbium L_{III} absorption edge energy (7506 eV), and the edge energy ± 100 eV. Data at the different energies were collected cyclically, for 300 s at each energy value, such that an absorption edge measurement always preceded and followed data collected at ±100 eV from the edge. After collecting data in the manner just described for a total time of 60 min, a UV-light flash (2–5 s) was used to photolize the caged ATP present in the sample and synchronously initiate phosphorylation of the ATPase-molecule ensemble; the duration of this UV-light flash was chosen to ensure the photolysis of 100% of the caged-ATP in the oriented multilayer specimens, as determined independently. After the UV flash, lamellar diffraction patterns were recorded using the same scheme employed before the flash.

X-ray diffraction data reduction and analysis

The "raw" two-dimensional diffraction data files were integrated perpendicular to the lamellar z^*-axis over a strip, whose width was sufficient to include the extent of the lamellar diffraction in this direction due to the x-ray beam's partial focus in this direction and the multilayer sample's mosaic spread (layer misorientation), to thereby reduce them to one-dimensional lamellar intensity functions $I_0(c, E)$ (where c denotes the channel number to which the counts were assigned by the detector's position decoding circuit, and E denotes the x-ray energy at which the pattern was collected) that were then transferred to a VAX 11–750 computer (Digital) for further analysis. For every set of $I_0(c, E)$ lamellar intensity functions, the position in channel number of the reciprocal space origin ($z^* = 0$) was determined, and the detector channel coordinate was converted to the reciprocal space coordinate $z^* = (2\sin\theta)/\lambda$. For off-edge (±100 eV) energy diffraction patterns, the intensity versus z^* data were interpolated to match the z^* values corresponding to the edge energy patterns. Finally, all $I_0(z^*, E)$ functions in a data set were normalized to the same total integrated (over an identical z^*-range) intensity, to account for variations due mostly to the decreasing synchrotron ring current during the course of an experiment. This normalization also resulted in all patterns from a set having identical lamellar background scattering, independently of their x-ray energy. To ensure further that no artifacts due to sample instability were present in the data, every pair of normalized, one-dimensional lamellar intensity functions originating from consecutive two-dimensional data files in both the pre- and post-UV flash data sets from a given sample were compared via subtraction to check for sample instabilities. Only consecutive edge-energy patterns for which no time-dependent changes could be observed, and the off-edge energy patterns included between them, were used for further analysis. For both the pre- and post-UV flash data sets, files that satisfied the preceding stability criteria were then added together to improve the counting statistics, according to their x-ray energy. This resulted in three pre-UV and three post-UV flash lamellar intensity functions $[I_0(z^*, E_{edge}), I_0(z^*, E_{edge\pm\Delta})]$ per sample, which were then corrected to account for the estimated lamellar background scattering by subtracting precisely the same piecewise-continuous exponential approximation to the background scattering function (Asturias and Blasie, 1991). A Lorentz correction proportional to z^* was also applied (to account for the cylindrical curvature of the multilayer samples) to obtain the corresponding background-corrected intensity functions $[I_c(z^*, E_{edge}), I_c(z^*, E_{edge\pm\Delta})]$. Only the edge-energy lamellar intensity functions were used for further analysis of the time-resolved, nonresonance x-ray diffraction data described in *this* paper. (Note: Generally, off-resonance lamellar x-ray diffraction data collected "far" from an absorption edge of any element in the hydrated SR membrane would be employed for such a nonresonance analysis. However, the utilization of any lamellar x-ray diffraction data collected at *constant* x-ray energy at or near the absorption edge of interest for the resonance analysis minimizes the possibilty of systematic error in the comparision between electron density profiles derived in the nonresonance analysis and those derived from the resonance analysis, as in the accompanying paper. Furthermore, the resonant metal atoms bound to the metal-binding/transport sites on the SR Ca^{2+}ATPase are so small in number compared with the nonresonant atoms in the hydrated SR membrane that they make virtually no contribution to the membrane electron density profile unless detected specifically via a resonance experiment.) The lamellar diffraction data extended to $z^*_{max} = 0.0425$ Å^{-1}, corresponding to a spatial resolution of ~23 Å in the derived multilayer unit cell electron density profiles.

Pre- and post-UV flash multilayer unit cell electron density profiles were calculated from the $I_c(z^*, E_{edge})$ data using the General Fourier Synthesis Deconvolution Method of analysis (GFSDM) (Schwartz et al., 1975). The changes in the unit cell electron density profile induced by flash photolysis of caged ATP and subsequent enzyme phosphorylation were calculated by taking the direct arithmetic difference between the pre- and post-UV flash profiles. To further check this result, the difference lamellar intensity function, $\Delta[I_c(z^*, E_{edge})] = [I_c^{1/2}(z^*, E_{edge})_{post\text{-}UV} - I_c^{1/2}(z^*, E_{edge})_{pre\text{-}UV}]^2$, was subjected to direct analysis, assuming the phosphorylation-induced changes in the unit cell electron density profile to be small, using the Box Refinement Method (Stroud and Agard, 1979), which was "biased" to produce a centrosymmetric, difference unit cell electron density profile. Finally, the pre- and post-UV flash multilayer unit cell electron density profiles were fit with step-function electron density models to facilitate the interpretation of the

changes induced by enzyme phosphorylation in terms of the SR membrane's molecular components.

RESULTS

Enzyme phosphorylation level and E~P lifetime measurements in the presence of lanthanides

Measurements of the level of phosphorylation of the Ca^{2+}ATPase and the lifetime of the phosphorylated enzyme intermediate, in the presence of lanthanides, were undertaken to confirm (under conditions more relevant to our x-ray diffraction studies) previous reports on the capacity of lanthanides to activate the Ca^{2+}ATPase for phosphorylation (Squier et al., 1990), and also to serve as a guide in the design of the x-ray diffraction experiments.

First, we compared the capacity of lanthanum versus calcium to activate enzyme phosphorylation at 4°C, employing conditions otherwise similar to those reported in the literature (Squier et al., 1990) at a temperature of ~20°C. For these experiments, the $[Ca^{2+}]$/[ATPase] mole ratio was 5:1, the $[La^{3+}]$/[ATPase] mole ratio was 10:1, the $[Mg^{2+}]$/[ATPase] mole ratio was either 1:1 or 1000:1, and ATP was in excess at a [ATP]/[ATPase] mole ratio of 100:1. The main results from these first experiments are shown in Fig. 1 *A* for $[Mg^{2+}]$/[ATPase] ≅ 1:1. As evidenced by the data presented in Fig. 1 *A*, the presence of lanthanum produces a dramatic change in the lifetime of the phosphorylated enzyme. At 4°C, for phosphoenzyme formed in the presence of Ca2+ but in the absence of La^{3+}, the phosphoenzyme level has already dropped to less than 50% of the maximum level after only ~90 s (this maximum level in the presence of Ca^{2+} is typically ~50% phosphoenzyme, which is reached in <30 s) (Fig. 1 *A*). On the other hand, for phosphoenzyme formed in the presence of La^{3+}, after ~40 min, the phosphoenzyme level has only dropped to 75% of the maximum level (this maximum level is typically ~25% phosphoenzyme in the presence of La^{3+}, which is reached in ~60 s) (Fig. 1 *A*). The maximum level of phosphoenzyme formation is somewhat dependent on the $[Mg^{2+}]$/[ATPase] mole ratio under the conditions of these experiments, increasing to ~70% phosphoenzyme for Ca^{2+}-activated phosphorylation and ~35% for La^{3+}-activated phosphorylation for a $[Mg^{2+}]$/[ATPase] ratio of ~1000/1. These results, obtained in the presence of excess ATP, indicate that lanthanum can effectively activate the enzyme for phosphorylation and greatly extend the lifetime of the phosphorylated enzyme intermediate at 4°C, as already suggested by earlier room temperature (~20°C) measurements described in the literature (Squier et al., 1990).

Second, we investigated the capacity of terbium, instead of lanthanum, to activate enzyme phosphorylation at 4°C, and under conditions much more closely approximating those in the oriented multilayers utilized in the x-ray diffraction experiments. Tb^{3+} was used instead of La^{3+} for the x-ray diffraction experiments because of the higher energy location of its L_{III} absorption edge, and also because of its higher capacity to displace Ca^{2+} from the high-affinity binding/transport sites on the ATPase protein (see Discussion). For these experiments, we utilized $[Tb^{3+}]$/[ATPase] mole ratios of 10:1 and 5:1, $[Mg^{2+}]$/[ATPase] mole ratios of 5:1 and 2500:1, and limiting ATP at a mole ratio of [ATP]/[ATPase] ≅ 5:1. The results of these experiments are shown in Fig. 1 *B*. As evidenced by the data presented in Fig. 1 *B*, the presence of terbium also produces a dramatic change in the lifetime of the phosphorylated enzyme, as compared with calcium. At 4°C, the phosphoenzyme level decays to only ~60% of its maximum level (~8% phosphoenzyme) after 60 min for a $[Mg^{2+}]$/[ATPase] mole ratio of 5:1; for a much higher $[Mg^{2+}]$/[ATPase] mole ratio of 2500:1, the phosphoenzyme level decays to ~25% of its maximum level (~25% phosphoenzyme) after about 20 min. The conditions present in the oriented multilayers utilized in the x-ray diffraction experiments were most likely intermediate (based on the expected ratios of Mg^{2+}·ATP to Tb^{3+}·ATP available for

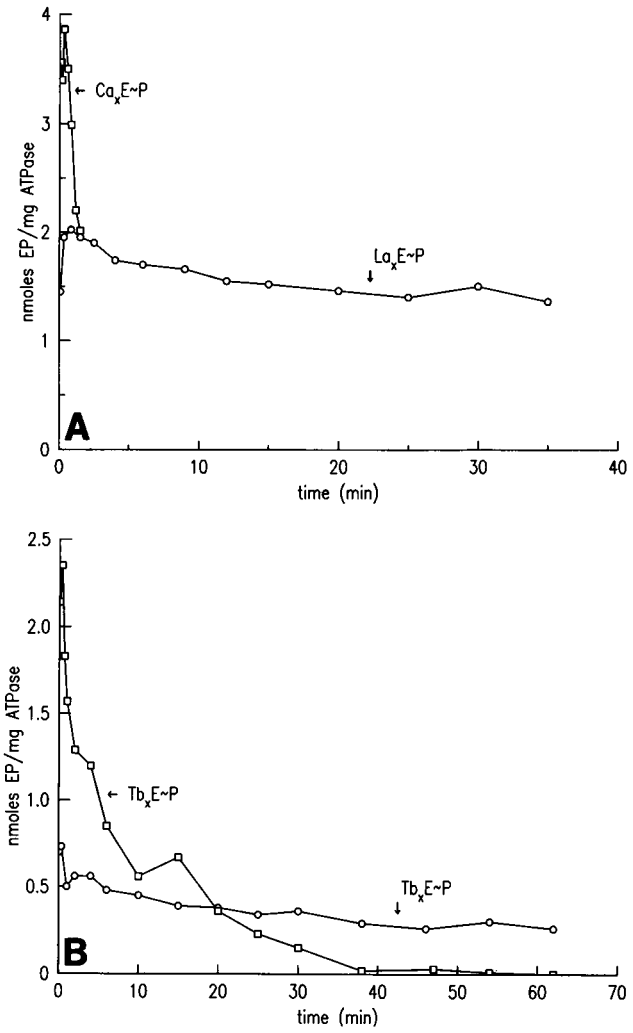

FIGURE 1 Phosphoenzyme formation and decay at 4°C. (*A*) Ca^{2+} versus La^{3+} activation of phosphoenzyme formation. Reaction conditions were 80 mM KCl, 20 mM MOPS pH 6.85, 400 μM ATP, 4 μM ATPase, 4 μM Mg^{2+}, and either 20 μM Ca^{2+} (□) *or* 40 μM La^{3+} (○). (*B*) Tb^{3+} activated enzyme phosphorylation under two sets of conditions that bracket those of the x-ray diffraction experiments. Reaction conditions were 100 mM KCl, 20 mM MOPS (pH 6.85), 20 μM ATP, 4 μM ATPase, and either 40 μM Tb^{3+} and 20 μM Mg^{2+} (○) *or* 20 μM Tb^{3+} and 10 mM Mg^{2+} (□).

binding at the enzyme's catalytic site under the conditions of the enzyme phosphorylation, as compared with the x-ray diffraction, experiments (see Discussion)) between the two extremes of $[Mg^{2+}]$/[ATPase] mole ratio shown in Fig. 1 *B*.

X-ray diffraction measurements: calculation of pre- and post-UV flash $\rho_{uc}(z)$, and $\Delta\rho_{uc}(z)$

Data from the x-ray diffraction experiments collected at 4°C were subjected to preliminary evaluation according to the criteria described in Materials and Methods, and then analyzed as also described. The specimens examined showed very reproducible changes in their lamellar diffraction upon the flash photolysis of caged ATP in the oriented multilayer, i.e., upon terbium-activated enzyme phosphorylation. A typical lamellar diffraction function $I_0(z^*, E_{edge})$, as well as the changes observed in this function upon photolysis of caged ATP, are shown in Fig. 2. Entirely similar results were obtained with lanthanum activation of enzyme phosphorylation and CuKα x-rays (8088 eV) from a rotating-anode x-ray source (Asturias and Blasie, 1989; Asturias et al., 1990) under otherwise similar conditions. The GFSDM-calculated multilayer unit cell electron density profiles before ($\rho^{E}_{uc}(z)$) and ($\rho^{E\sim P}_{uc}(z)$) after flash photolysis of caged ATP and enzyme phosphorylation are shown in Fig. 3; in addition, their difference ($\rho^{E\sim P}_{uc}(z)$) – ($\rho^{E}_{uc}(z)$) multiplied by a factor of 2 is also shown in Fig. 3. As can be seen in Fig. 3, significant changes in the electron density profile of the SR membrane are observed upon terbium-activated phosphorylation of the ATPase protein. The changes are most significant

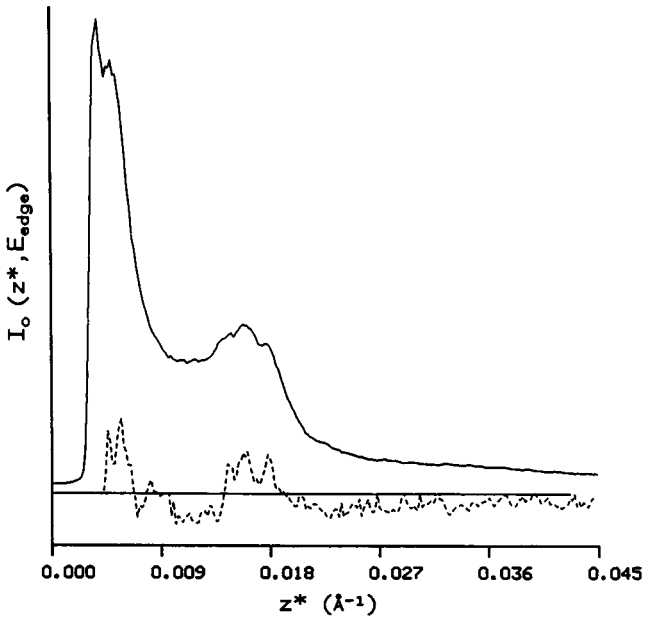

FIGURE 2 Uncorrected lamellar x-ray diffraction $I_0(z^*, E_{edge})$ from an oriented, partially dehydrated SR multilayer, and the changes observed in the diffraction (- - - -) upon phosphorylation of the Ca^{2+}ATPase, activated by terbium and initiated via the flash photolysis of 100% of the caged ATP present in the oriented multilayer. The changes in the lamellar diffraction are shown in the figure at 20 times that observed.

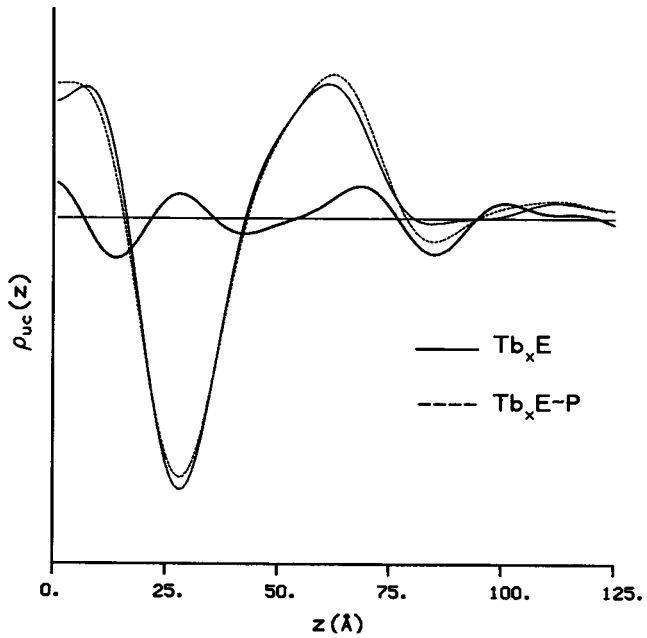

FIGURE 3 The SR membrane relative electron density profile before (Tb_xE, ———) and immediately after ($Tb_xE\sim P$, - - - -) Tb^{3+}-activated phosphorylation of the Ca^{2+}ATPase protein. The difference between the profiles ($Tb_xE\sim P$ *minus* Tb_xE) is also shown (the difference profile is shown at 2 times the actual values). The profiles were calculated using the Generalized Fourier Synthesis Deconvolution Method (GFSDM). Note that significant changes occur throughout the SR membrane profile upon terbium-activated enzyme phosphorylation.

in the regions centered about $z \cong 5$ Å, $z \cong 30$ Å, and $z \cong 70$ Å. Fitting these unit cell electron density profiles with step-function electron density models facilitates the interpretation of the observed changes in terms of the membrane's molecular components. This modeling is described in the next section.

Multilayer electron density profiles, such as those in Fig. 3, are in general very sensitive to the phasing of the lamellar x-ray diffraction data; the GSFDM solution to the phase problem (Schwartz et al., 1975) has been demonstrated (over the past two decades) to be a reliable method for solving the phase problem for multilayer systems exhibiting lattice disorder of the so-called second kind. The phases assigned by the GFSDM analysis to each one of the constant phase regions in $I_c(z^*, E_{edge})$ are shown in Table 1, and compared with the phases obtained from analysis of lamellar intensity functions collected from oriented SR multilayer samples under a number of different physicochemical conditions. Note that the phases assigned to the present data agree with the phases determined to be correct for lamellar intensity functions recorded under conditions that slow the formation and extend the lifetime of the phosphorylated enzyme intermediate $M_xE\sim P$ (Asturias and Blasie, 1989; Asturias et al., 1990), such as low $[Mg^{2+}]$ and temperatures below t_h (the characteristic temperature for reversible lateral phase separation of the membrane lipids; see Discussion for more details). As indicated under Materials and Methods, the changes in the unit cell electron density profile induced by phosphorylation

TABLE 1 Influence of temperature and metal ion concentration on the phases assigned to the lamellar x-ray diffraction maxima from oriented SR membrane multibilayers

Conditions	Phase assignment
25 mM $[Mg^{2+}]$, $T > t_h$	++−
25 mM $[Mg^{2+}]$, $T < t_h$	−+−
100 μM $[Mg^{2+}]$,	−+−
La/Tb^{3+}	−+−

The first constant phase region includes the first diffraction order, the second constant phase region includes orders 2 through 5, and the third region includes orders 6 and 7. All the conditions that slow the formation and decay of the phosphorylated enzyme intermediate $M_xE\sim P$, such as low temperature, low $[Mg^{2+}]$, or the presence of lanthanides replacing calcium (Asturias and Blasie, 1991), also cause a reversal in the phase of the first-order diffraction maximum (+ → −).

of the Ca^{2+}ATPase in the presence of Tb^{3+} were also calculated by subjecting the change upon protein phosphorylation in the lamellar intensity function $\Delta I_c(z^*, E_{edge})$ as defined above, to Box Refinement analysis. The change in the unit cell electron density profile calculated by Box Refinement and the change calculated by taking the difference between the GFSDM-calculated electron density profiles before and after protein phosphorylation are in agreement (results not shown), which confirms the phase assignment obtained via the GFSDM analysis of the data.

Modeling of $\rho^{E}_{uc}(z)$ and $\rho^{E\sim P}_{uc}(z)$ membrane electron density profiles

Fitting of step-function electron density models to the continuous unit cell electron density profiles for the unphosphorylated ($\rho^{E}_{uc}(z)$) and phosphorylated ($\rho^{E\sim P}_{uc}(z)$) enzyme conformations allows interpretation of the observed changes in the profile structure of the membrane in terms of the membrane's molecular components. We have previously applied this method of analysis to study and interpret changes in the SR membrane profile induced by different physicochemical parameters, such as temperature and ionic strength (Asturias and Blasie, 1989; Pascolini and Blasie, 1988), as well as changes observed upon Ca^{2+}-activated phosphorylation of the ATPase (Blasie et al., 1985; Pascolini and Blasie, 1988). The minimum number of steps required to model the continuous unit cell electron density profile was used, namely nine steps for each half of the centrosymmetric unit cell profile containing the apposed pair of SR single membrane profiles. All steps were assigned a width of 14 Å, consistent with the limited spatial resolution (~20 Å) to which the continuous profiles were calculated. The two adjacent steps at the center of the unit cell profile, which represent the electron density corresponding to the intravesicular water space between the two apposed membranes, overlap to form a single narrow strip, 10 Å wide.

The fit of the step-function model profile was tested and optimized by (a) comparing the model profile's unit cell structure factor modulus square $|F_{uc}(z^*)|^2$ with the corresponding experimental function obtained from the GFSDM analysis of the experimental data, and (b) calculating the Fourier transform of the step-function model profile, truncating in z^* to match the truncation window in the experimental data, and then back-transforming to obtain the continuous electron density model profile corresponding to the step electron density model, which was then compared directly with the experimental unit cell electron density profile obtained from the GFSDM analysis. The former represents a traditional "model refinement analysis" *without* phase information, whereas the latter represents a "real space refinement" analysis *with* phase information. The unit cell structure factor modulus square $|F_{uc}(z^*)|^2$ (residual[2] $R_F = 1.03 \times 10^{-3}$) and continuous unit cell electron density profile for the refined step-function electron density model profile, as well as the corresponding experimental functions obtained from the GFSDM analysis of the data for the unphosphorylated enzyme conformation (Tb_xE), are shown in Fig. 4. Similar results were obtained in the case of the phosphorylated ($Tb_xE\sim P$) enzyme conformation. Fig. 5 shows the refined step-function electron density model profiles for the experimental unit cell electron density profiles corresponding to the unphosphorylated and phosphorylated enzyme conformations.

In carrying out the "real space refinement" analysis described above, the amplitudes of the different electron density steps in the model profile were changed by progressively smaller amounts. Uncertainty in the amplitude of the steps was thereby found to vary between 2 and 10%. The uncertainty is larger for steps that represent a small value of the relative electron density, because variations in the amplitude of such steps have only a small, but localized effect on the continuous relative electron density profile corresponding to the step-function model, and an even lesser, delocalized effect on its corresponding unit cell structure factor modulus.

The results from previous x-ray and neutron diffraction studies make it possible to identify unequivocally the specific regions within the SR membrane profile represented by the different steps in the models shown in Fig. 5 (Herbette et al., 1985; Pascolini et al., 1988; Pascolini and Blasie, 1988). Two steps (2 and 5) correspond to the phospholipid polar headgroup regions at the intravesicular and extravesicular surfaces of the membrane, respectively. Steps 3 and 4 correspond to the acyl chain regions of the inner and outer monolayer, respectively, of the membrane's lipid bilayer. Five steps (6 through 10) correspond to the extravesicular portion of the membrane profile, extending to the edge of the unit cell. Finally, step 1 represents the intravesicular water space. The "transbilayer" portion of the Ca^{2+}ATPase occurs within steps 2–4, the "stalk" portion within step 5 and the "headpiece" portion of the ATPase in steps 6–8. As can be seen from Fig. 5, upon terbium-activated phosphorylation of

[2] The residuals for a given function $f(x)_{calc}$ were calculated as

$$R_f = \sum [f(x)_{calc} - f(x)_{exp}]^2 / \sum [f(x)_{exp}]^2$$

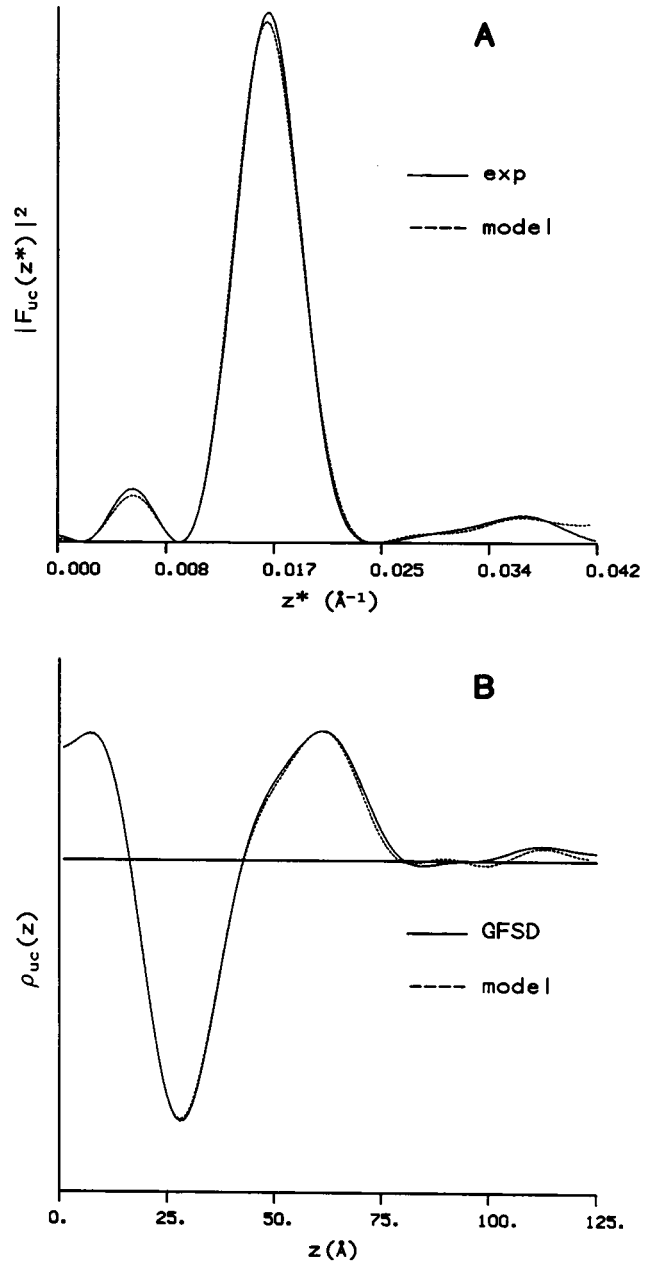

FIGURE 4 Refinement of the step-function model profile for the SR membrane relative electron density profile before enzyme phosphorylation. The fit of the step-function electron density model profile was optimized by minimizing the difference between experimental GFSDM-calculated and corresponding model functions. (*A*) Unit cell structure factor modulus square $|F_{uc}(z^*)|^2$ (residual^2 $R_F = 1.03 \times 10^{-3}$) and (*B*) continuous, single membrane relative electron density profile for the refined step-function model profile as compared with the corresponding functions obtained from the GFSDM analysis of the experimental data. Similar results were obtained for the terbium-activated, phosphorylated enzyme conformation.

the ATPase protein, there are "large-scale" (i.e., long-range) structural changes throughout the SR membrane profile, specifically a small, but significant, increased electron density in steps 1, 3, 6, and 8 and a small, but significant, decreased electron density in steps 2, 4, 5, and 7.

DISCUSSION

Protein phosphorylation and phosphoenzyme lifetime in the presence of La^{3+} or Tb^{3+}: interaction of lanthanides with the Ca^{2+}ATPase

Our studies of enzyme phosphorylation and phosphoenzyme lifetime in the presence of La^{3+} and Tb^{3+}, as compared with Ca^{2+}, provide some information concerning the nature of the interaction of lanthanides with the Ca^{2+}ATPase from SR, and their effect on its functionality. *Low* lanthanide concentrations (lanthanide/ATPase mole ratios 5–10) were used to ensure saturation of the high-affinity metal-binding sites on the enzyme while also minimizing the extent of nonspecific binding of lanthanide ions to the SR membrane components and, therefore, any effects that this nonspecific binding might have on the membrane structure and functionality (e.g., the presence of excess lanthanide ions could cause extensive lateral phase separation of the membrane lipids and thereby affect the functionality of the ATPase). There are several reports in the literature (Squier et al., 1990; Girardet et al., 1989; Hanel and Jencks, 1990) that indicate that lanthanides bind to a number of different protein sites, including high-affinity calcium-binding/transport sites on the ATPase. Evidence that, under certain conditions, lanthanides bind to calcium-binding/transport sites on the enzyme is provided by measurements of the stoichiometry and affinity of lanthanide binding, the nature of changes in the intrinsic fluorescence of tryptophan residues in the Ca^{2+}ATPase upon displacement of Ca^{2+} by lanthanides, and from the results of lanthanide "chase" experiments using ^{45}Ca (Squier et al., 1990; Girardet et al., 1989). The affinity of binding to the calcium sites depends on the particular lanthanide involved. Terbium seems to be more efficient than lanthanum at displacing Ca^{2+} from the high-affinity binding-transport sites (Squier et al., 1990). For Tb^{3+}, the values reported for the dissociation constant for these sites range from 16 (Squier et al., 1990) to 10 nM (Girardet et al., 1989), whereas values for La^{3+} appear to be larger by roughly an order of magnitude (Squier et al., 1990). A complication arises for *high* lanthanide/ATPase mole ratios, in the absence of specific lanthanide-buffering agents, namely that the apparent dissociation constant for lanthanides from the high-affinity calcium-binding/transport sites is 2–4 times larger than that for Ca^{2+} (Squier et al., 1990; Girardet et al., 1989), which has been attributed to the occurrence of nonspecific binding of the lanthanides to the SR membrane.

The results presented in Fig. 1 *A* confirm earlier reports (Squier et al., 1990) that, in the presence of lanthanum as compared with calcium, the Ca^{2+}ATPase protein is phosphorylated to a significant level and that the lifetime of the phosphoenzyme is dramatically extended from <200 s to >40 min at 4°C, utilizing excess ATP. The maximum level of enzyme phosphorylation varies from 25 to 35% as the $[Mg^{2+}]$/[ATPase] mole ratio is varied over three orders of magnitude from 1:1 to 1000:1, respectively. The results shown in Fig. 1 *B* demonstrate that the enzyme is also

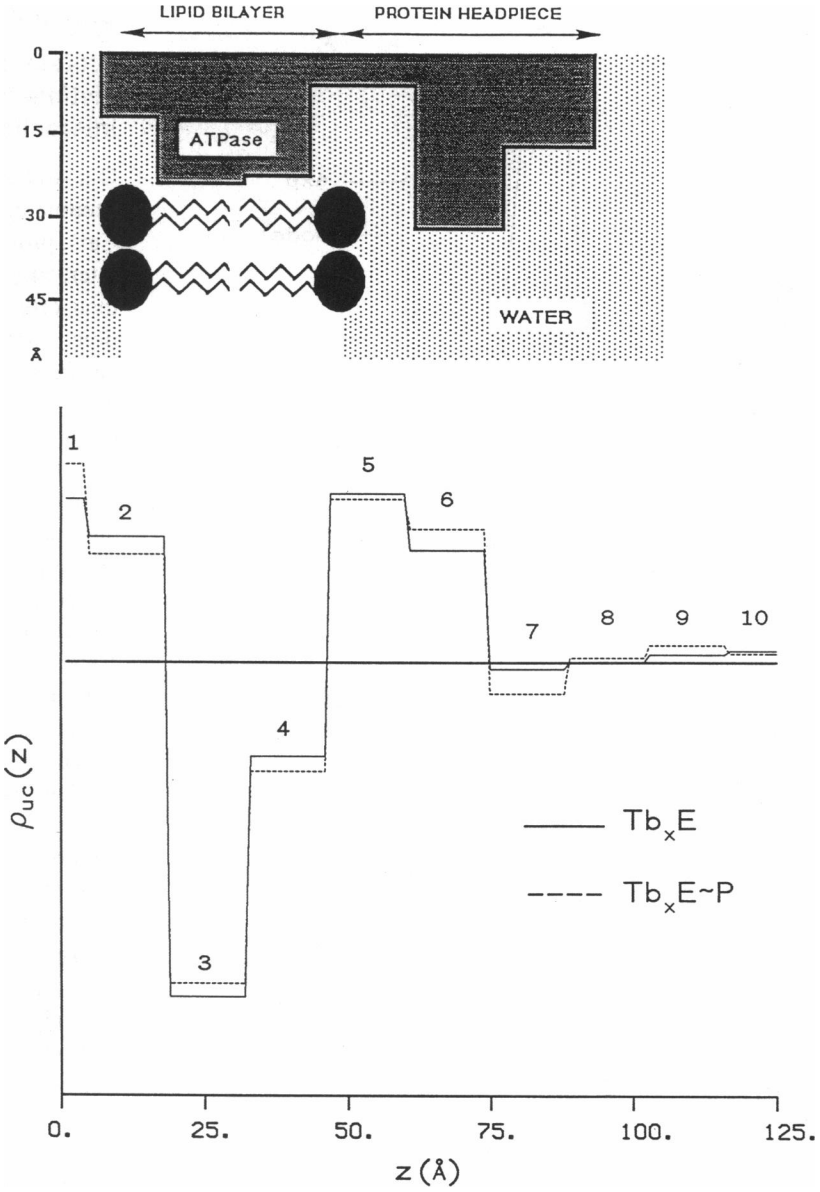

FIGURE 5 Refined step-function electron density electron density model profiles of the SR membrane before (Tb_xE, ———), and immediately after ($Tb_xE{\sim}P$, - - - - -) Tb^{3+}-activated phosphorylation of the Ca^{2+}ATPase protein. Two steps (2 and 5) correspond to the intra- and extravesicular phospholipid polar head group regions of the SR membrane profile, respectively. Steps 3 and 4 correspond to the acyl chain regions of the inner and outer monolayer of the membrane's lipid bilayer, respectively. Five steps (6–10) correspond to the extravesicular portion of the membrane profile, extending to the edge of the unit cell. Finally, step 1 represents the intravesicular water space. A schematic representation of the SR membrane profile is included for reference. Note that, as observed for the continuous profiles shown in Fig. 3, the significant changes in the profile structure of the membrane induced by phosphorylation of the ATPase protein occur throughout the membrane profile including the intravesicular surface of the membrane (steps 1 and 2), the acyl chain region of the membrane's lipid bilayer (steps 3 and 4), and the "headpiece" region of the Ca^{2+}ATPase protein (steps 6 and 7).

phosphorylated to a somewhat lesser, but significant level in the presence of terbium and that the lifetime of the phosphoenzyme is also dramatically extended to >20 min at 4°C. In this case, the maximum level of enzyme phosphorylation varies from 8 to 25% as the $[Mg^{2+}]$/[ATPase] mole ratio is varied over nearly three orders of magnitude, from 5:1 to 2500:1, respectively. The conditions for these experiments, with Tb^{3+} as the activating metal cation and with very limiting ATP, closely resemble the conditions in the oriented SR multilayers employed in the x-ray diffraction experiments. It should be noted that it is primarily this dramatic extension of the phosphoenzyme lifetime in the presence of lanthanum or terbium that makes possible the time-resolved, resonance x-ray diffraction experiments described in the accompanying paper (Asturias et al., 1993). Also, the higher x-ray energy of the lanthanide L-absorption edges, as opposed to the lower-energy calcium K-edge, facilitates the resonance x-ray diffraction experiments.

The results from our x-ray diffraction experiments provide further evidence that supports the results from our enzyme phosphorylation and phosphoenzyme lifetime measurements. The changes in the lamellar diffraction function $I_0(z^*, E_{edge})$ (Fig. 2), observed upon flash photolysis of caged ATP in the oriented SR membrane multilayer samples, confirm the results concerning the significant level of enzyme phosphorylation and the dramatic extension of the lifetime of the phosphorylated enzyme conformation when terbium acts as the activating metal ion bound to the high-affinity transport sites in the enzyme. Given the time-frame of the diffraction experiments (*total* data collection time after the flash photolysis of caged ATP was 50–60 min), no significant changes in $I_0(z^*, E_{edge})$ would have been observed unless a significant fraction of the ATPase molecules had been phosphorylated, *and* unless the lifetime of the phosphorylated enzyme conformation had been extended to a time roughly comparable to this total x-ray data collection time (the limiting amount

of ATP present in the multilayer sample after photolysis of caged ATP could have only supported two turnovers of the ensemble of ATPase molecules).

It has also been suggested that the effect of lanthanides on the lifetime of the phosphorylated enzyme intermediate is not due to binding of the high-affinity calcium-binding/transport sites, but to replacement of Mg^{2+} by La^{3+} as the metal ion present at the catalytic site (Fujimori and Jencks, 1990). Under the conditions present in the oriented multilayers utilized for the x-ray diffraction experiments, we believe (see below) that the ratio of magnesium to terbium available for complexation with ATP, namely $[Mg^{2+}]/[Tb^{3+}]_{free}$, was about 500:1. Thus, the conditions in the oriented multilayers would be intermediate between the two sets of conditions shown in Fig. 1 *B*. (The pure SR dispersions utilized to form the oriented multilayers contained [ATPase] $\cong 10^{-5}$ M, $[Tb^{3+}] \cong 4 \times 10^{-5}$ M, $[Mg^{2+}] \cong 10 \times 10^{-3}$ M, and [c-ATP] $\cong 5 \times 10^{-3}$ M. If one assumes, as is generally accepted, that there are two single-occupancy, high-affinity metal-binding sites on the ATPase and utilizes the established twofold increase in the concentration of solutes *not bound* to the SR membrane upon sedimentation and partial-dehydration to form the oriented multilayers, the oriented multilayers would thereby contain [ATPase] $\cong 5 \times 10^{-3}$ M, $[Tb^{3+}]_{free} \cong 4 \times 10^{-5}$ M, $[Mg^{2+}] \cong 20 \times 10^{-3}$ M, and [c-ATP] $\cong 10 \times 10^{-3}$ M.) The dissociation constants for lanthanide-ATP complexes are smaller than the dissociation constant for Mg·ATP by roughly two orders of magnitude [~0.1 and ~10 μM, respectively at pH 7 (Girardet et al., 1989; Morrison and Cleland, 1983), and magnesium and lanthanide complexes bind to the ATPase with very similar affinities ($K_d \sim 3$ μM (Girardet et al., 1989))]. However, as indicated before, the dissociation constants for binding of lanthanides to the high-affinity binding/transport sites on the ATPase is of the order of ~0.01 μM for terbium to ~0.1 μM for lanthanum (Squier et al., 1990; Girardet et al., 1989). This suggests that, under our experimental conditions, the ATP would not compete very effectively for the terbium bound to the high-affinity sites on the ATPase in the oriented multilayers resulting in a $[Mg^{2+}]/[Tb^{3+}]_{free}$ ratio about 500:1. Given the above mentioned dissociation constants, this would result in a Mg^{2+}·ATP/Tb^{3+}·ATP ratio of ~5:1 and, thereby, primarily Mg^{2+}ATP at the catalytic site on the enzyme in the oriented multilayers. Furthermore, the results from our x-ray diffraction experiments provide evidence that, under the conditions of our measurements, the effect of lanthanides is most likely not due to their presence at the enzyme's catalytic site, but instead is due to their effect on the profile structure of the SR membrane (discussed in the following section) and to their presence at binding/transport sites on the ATPase (discussed in the accompanying paper (Asturias et al., 1994)).

Our results, when considered in conjunction with previous reports in the literature concerning the interaction of lanthanides with the Ca^{2+}ATPase, provide strong evidence to support the claim that, under the conditions of our experiments, lanthanides were indeed responsible for activating the ATPase for phosphorylation. Previously published results in the literature are sometimes conflicting, perhaps for a number of reasons, including differences in the type of SR preparation used for the experiments and, more likely, large variations in the range of lanthanide/protein mole ratios studied. Additional complications may arise from the fact that it is difficult to accurately control and measure very low lanthanide concentrations, especially given the propensity of lanthanides to bind or form complexes with a variety of organic and inorganic agents.

Changes in $\rho_{uc}(z)$ upon phosphorylation of the ATPase in the presence of Tb^{3+}: step-function electron density models

Significant changes are observed in the SR membrane relative electron density profile (contained in each half of the multilayer unit cell relative electron density profile $\rho_{uc}(z)$) upon phosphorylation of the Ca^{2+}ATPase protein in the presence of Tb^{3+} (i.e., upon the conversion $Tb_xE \rightarrow Tb_xE{\sim}P$). To facilitate the interpretation of these changes in the profile structure of the membrane in terms of the membrane's molecular components, the unit cell electron density profiles corresponding to the unphosphorylated (Tb_xE) and phosphorylated ($Tb_xE{\sim}P$) enzyme conformations were fit with step-function electron density model profiles, shown in Fig. 5. The small but significant changes induced by protein phosphorylation activated by terbium can thereby be seen to correspond to: (a) an increase in the electron density of the intravesicular water space region of the SR membrane profile (step 1) and a decrease in the electron density of the adjacent polar headgroup region of the inner phospholipid monolayer (step 2); (b) an increase in the electron density of the acyl chain region of the inner phosphoslipid monolayer (step 3) and a decrease in the electron density of the acyl chain region of the outer phospholipid monolayer (step 4); and (c) a decrease in the electron density of the polar headgroup region of the outer phospholipid monolayer (step 5) with an increase in the electron density of a portion of the protein "headpiece" (step 6) and a decrease in the adjacent portion of the "headpiece" (step 7). The "physiological" significance of the changes in the SR membrane electron density profile contained within $\rho_{uc}(z)$, observed upon Tb^{3+}-activated phosphorylation, can be assessed by comparing them with the corresponding changes observed upon phosphorylation of the ATPase activated by Ca^{2+}, *especially within the more conformationally restrictive region of the profile containing the membrane phospholipid bilayer* (i.e., steps 2–5). Refined step-function electron density model profiles of the SR membrane profile before and after phosphorylation of the ATPase activated by Ca^{2+} at two different temperatures (above and below t_h, the upper characteristic temperature for reversible lateral phase separation of the membrane lipids) are shown in Fig. 6. Comparison of the SR membrane electron density profiles presented in Fig. 5 (Tb^{3+}-activated phosphorylation) and Fig. 6 (Ca^{2+}-activated phosphorylation) indicates that, although the details of the changes in the enzyme "headpiece" region of membrane profile (steps 6–8) induced by

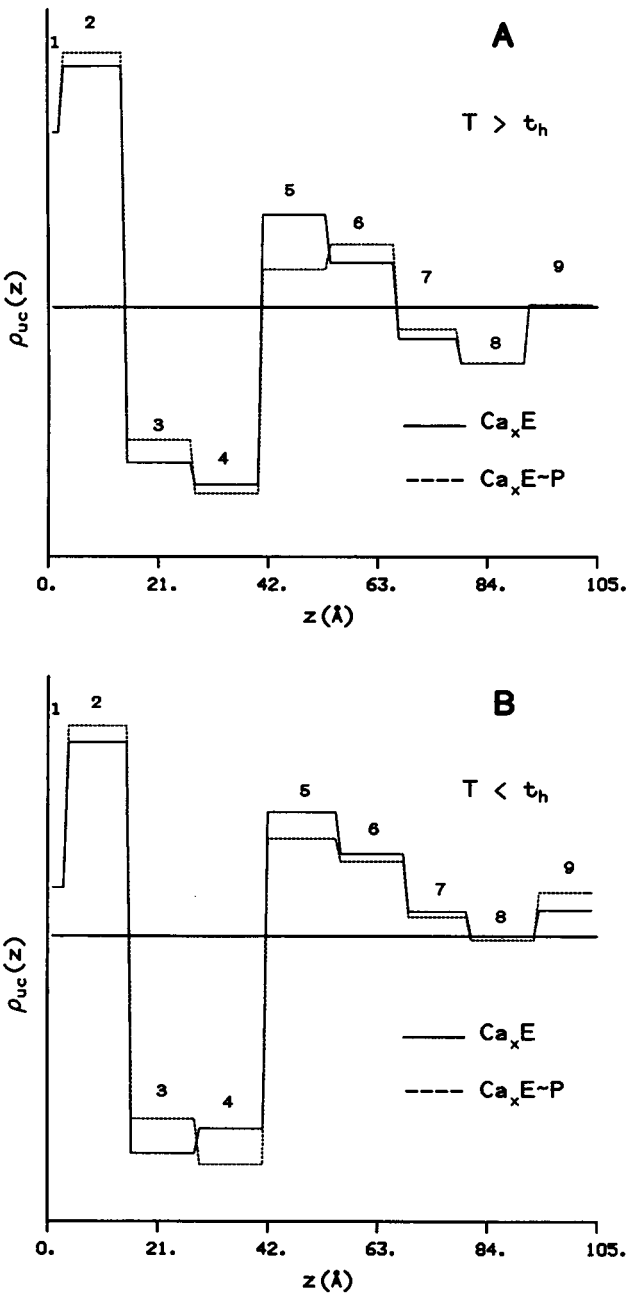

FIGURE 6 Refined step-function electron density model profiles of the SR membrane before (Ca_xE, ———), and immediately after (Ca_xE~P, - - - - -) Ca^{2+}-activated phosphorylation of the Ca^{2+}ATPase protein at temperatures above (*A*) and below (*B*) the upper characteristic temperature t_h for reversible lateral phase separation of the membrane lipids. The model refinement of the profiles was performed as described for the case of profiles corresponding to Tb^{3+}-activated protein phosphorylation (see Figs. 4 and 5 and text for details). Comparison with the step-function model profiles shown in Fig. 5 indicates the similarity of the changes observed upon Ca^{2+}- and Tb^{3+}-activated protein phosphorylation. See text for a discussion of these results.

phosphorylation of the ATPase differ depending on the particular conditions even for calcium activation, *the phosphorylation-induced changes within the phospholipid bilayer region of the membrane profile are extremely similar for all three cases, despite significant differences in the initial (i.e., before enzyme phosphorylation) profile structure of the membrane.* The latter changes include a decrease in electron density throughout the outer phospholipid monolayer region (steps 4 and 5) and an increase in electron density in the inner phospholipid monolayer region (steps 1–3) (note that step 1 is not actually distinguishable from step 2 because its width is substantially less than the resolution limit). We believe that this observation substantiates the relevance of our lanthanide-based structural studies to the elucidation of the mechanism of Ca^{2+} active transport. However, although Tb^{3+}-activated phosphorylation of the ATPase produces changes in the profile structure of the SR membrane that are qualitatively similar in nature to the changes observed upon Ca^{2+}-activated phosphorylation, especially within the more conformationally restrictive phospholipid bilayer region of the membrane profile, they are, in general, substantially smaller in magnitude within a particular step. This is most likely due to the lower level of enzyme phosphorylation achieved with lanthanides replacing calcium as the activating cation, as discussed in the preceding section.

Functional significance of lanthanide-induced changes in the profile structure of the SR membrane: lanthanides and the structure of the membrane lipids

We have reported the existence of a close correlation between the functionality of the Ca^{2+}ATPase and the structure of the SR membrane, in particular, the physical state of the membrane lipids (Asturias and Blasie, 1989; Asturias et al., 1990; Pascolini and Blasie, 1988). At temperatures below t_h (the upper characteristic temperature for reversible lateral phase separation of the membrane lipids), lateral phase separation of the membrane lipids is accompanied by a slowing of the formation, and a significant extension of the lifetime, of the phosphorylated enzyme conformation M_xE~P. Lateral phase separation of the membrane lipids is observed at lower multilayer hydration states, and at temperatures below t_h (whose value is influenced by the ionic compostion of the hydrating medium). Lateral phase separation of the membrane lipids can also be detected indirectly through its effect on the profile structure (as opposed to the in-plane structure) of the membrane. Conditions that cause lateral phase separation of the lipids and affect the kinetics of phosphoenzyme formation and decay produce changes in the lamellar diffraction from oriented SR multilayer samples. These changes are manifest by a reversal of the ratio of the amplitudes of the third and fourth order diffraction maxima, and by a reversal of the phase of the first order maxima (+ → −). This change in the phase of the first-order maxima has a profound effect on the profile structure of the membrane before enzyme phosphorylation, as can be seen by comparing the membrane step-function model electron density profiles shown in Fig. 6 *A* ($T > t_h$) and Fig. 6 *B* ($T < t_h$), most notaby a significant increase in the electron density of the acyl chain region of the outer phospholipid monolayer (step 4) relative to that of the inner monolayer (step 3). Thus, reversible lat-

eral phase separation of the membrane lipids is responsible for the occurrence of a transition in the SR membrane profile structure, which affects the membrane's functionality (Asturias et al., 1990). We have furthermore reported that the effect of $[Mg^{2+}]$ on the functionality of the ATPase, which some investigators (Yamada et al., 1986; Shigekawa et al., 1983) attributed to changes in the nature of the metal ion present at the catalytic site (Ca^{2+} replacing Mg^{2+} at low $[Mg^{2+}]$), can be explained, instead, by such changes in the structure of the membrane lipids mediated by changes in their degree of hydration caused by variations in $[Mg^{2+}]$ (Asturias et al., 1990). There have been other reports in the literature that point out the relationship between lipid structure and the functionality of the ATPase protein (Mendelsohn et al., 1984; Lentz et al., 1985; Moore et al., 1981; Bigelow and Thomas, 1987; Squier et al., 1988; Caffrey and Feigenson; 1981).

The effect of lanthanides on the functionality of the Ca^{2+}ATPase (slow formation, and very long lifetime of the phosphorylated enzyme conformation) can be viewed as an extrapolation of the effects of low temperature and/or low $[Mg^{2+}]$, which we have shown to be mediated by changes in the structure of the SR membrane. Although it has been proposed that the inhibition of steady-state turnover of the ATPase in the presence of lanthanides is due to the replacement of Mg^{2+} by lanthanides at the catalytic site (Hanel and Jencks, 1990; Fujimori and Jencks, 1990), this is most likely not the case under the conditions of our experiments, as discussed in an earlier section. Instead, we propose that the effect of lanthanides on the functionality of the Ca^{2+}ATPase is also mediated by changes in the structure of the SR membrane. The lamellar diffraction patterns from the Tb^{3+}-containing oriented multilayer samples analyzed in the present study are characteristic of SR multilayer samples in which the membrane lipids exhibit reversible lateral phase separation. As indicated in Results (see Table 1), the phase combination assigned to the lamellar diffraction data also agrees with that conclusion. Further evidence of the occurrence of lateral phase separation of the lipids is provided by examination of the step-function electron density model profiles shown in Fig. 5. Before enzyme phosphorylation, the electron density of the acyl chain region of the outer phospholipid monolayer (step 4) is substantially greater than that of the inner monolayer (step 3). The disparity in the electron density of these two steps is even greater than for the corresponding steps in Fig. 6 *B*, which shows the effect of lipid lateral phase separation on the SR membrane profile in the presence of calcium and high $[Mg^{2+}]$. The increased electron density of the acyl chain region in the outer monolayer most likely arises directly from lipid phase separation within this monolayer because domains of frozen acyl chains would possess a higher packing density of chains (i.e., smaller area/chain) in the membrane plane. We note, in this regard, that our previous resonance x-ray diffraction studies of the SR membrane profile, employing lanthanum to replace calcium on the Ca^{2+}ATPase's binding/transport sites at a La^{3+}/ATPase mole ratio of ~4, identified a minor, low-occupancy La^{3+} binding site in the phospholipid polar headgroup region of the outer monolayer in the SR membrane profile (Asturias and Blasie, 1991).

CONCLUSION

We have reported that, at low lanthanide/protein molar ratios (~5–10), lanthanides can activate phosphorylation of the Ca^{2+}ATPase in the SR membrane to an extent of 20–35% of that observed for calcium activation under similar conditions. The changes in the profile structure of the SR membrane observed upon phosphorylation of the ATPase protein are qualitatively similar in nature, but smaller in magnitude, for lanthanide versus calcium activation of enzyme phosphorylation. This similarity indicates that the results from our structural studies of the SR membrane using lanthanides as Ca^{2+} analogs are indeed relevant to the elucidation of the mechanism of Ca^{2+} active transport by the ATPase enzyme. We have also presented evidence that indicates that the effects of lanthanides on the functionality of the Ca^{2+}ATPase may be mediated by changes in the structure of the SR membrane, triggered by the presence of lanthanides. The results from the present study complement the results from a time-resolved, resonance x-ray diffraction study demonstrating that the changes in the profile structure of the SR membrane induced by lanthanide-activated phosphorylation of the Ca^{2+}ATPase result in a redistribution of lanthanide ions among the metal-binding sites previously identified in the membrane profile by resonance x-ray diffraction. The results from the time-resolved, resonance x-ray diffraction study are reported in an accompanying paper.

We are especially grateful to Prof. Giuseppe Inesi (University of Maryland School of Medicine, Baltimore, MD) for allowing us to perform the enzyme phosphorylation studies in his laboratories.

This work was supported by National Institutes of Health grants HL-18708. project#2 and RR01633 to J. K. Blasie.

REFERENCES

Asturias, F. J., and J. K. Blasie. 1989. Effect of Mg^{2+} concentration on Ca^{2+} uptake kinetics and structure of the sarcoplasmic reticulum membrane. *Biophys. J.* 55:739–753.

Asturias, F. J., and J. K. Blasie. 1991. Location of high-affinity metal binding sites in the profile structure of the Ca^{2+}ATPase in the sarcoplasmic reticulum by resonance x-ray diffraction. *Biophys. J.* 59:488–502.

Asturias, J. Francisco, R. F. Fischetti, and J. K. Blasie. 1994. A time-resolved, resonance x-ray diffraction study of changes in the relative occupancy of metal-binding sites in the profile structure of the sarcoplasmic reticulum membrane induced by phosphorylation of the Ca^{2+}ATPase enzyme in the presence of terbium. *Biophys. J.* 66: 1665–1677.

Asturias, F. J., D. Pascolini, and J. K. Blasie. 1990. Evidence that lipid lateral phase separation induces functionally significant structural changes in the Ca^{2+}ATPase of the sarcoplasmic reticulum. *Biophys. J.* 58:205–217.

Bigelow, D., and D. Thomas. 1987. Rotational dynamics of lipid and the Ca^{2+}ATPase in sarcoplasmic reticulum. *J. Biol. Chem.* 262:13449–13456.

Blasie, J. K., D. Pascolini, F. J. Asturias, L. Herbette, D. Pierce, and A. Scarpa. 1990. Large-scale structural changes in the sarcoplasmic reticulum ATPase appear essential for calcium transport. *Biophys. J.* 58: 687–693.

Blasie, J. K., L. Herbette, D. Pascolini, V. Skita, D. Pierce, and A. Scarpa.

1985. Time-resolved x-ray diffraction studies of the sarcoplasmic reticulum membrane during active transport. *Biophys. J.* 48:9–18.

Blasie, J. K., L. Herbette, and J. Pachence. 1985. Biological membrane structure as "seen" by x-ray and neutron diffraction. *J. Membr. Biol.* 86:1–7.

Caffrey, M., and G. W. Feigenson. 1981. Fluorescence quenching in model membranes. 3. Relationship between calcium adenosinetriphosphate enzyme activity and the affinity of the protein for phosphatidylcholines with different acyl chain characteristics *Biochemistry.* 20:1949–1961.

Clarke, D., D. Maruyama, T. Loo, E. Leberer, G. Inesi, and D. MacLennan. 1989. Functional consequences of glutamate, aspartate, glutamine, and asparagine mutations in the stalk sector of the Ca^{2+}ATPase of sarcoplasmic reticulum. *J. Biol. Chem.* 264:11246–11251.

Clarke, D., T. Loo, G. Inesi, and D. MacLennan. 1989. Location of high affinity Ca^{+2} sites within the predicted transmembrane domain of the sarcoplasmic reticulum Ca^{+2}ATPase. *Nature (Lond.).* 339: 476–478.

Dupont, Y. 1980. Occlusion of divalent cations in the phosphorylated calcium pump of sarcoplasmic reticulum. *Eur. J. Biochem.* 109:231–238.

Dupont, Y., F. Guillaing, and J. Lacapere. 1988. Fluorimetric detection and significance of conformational changes in Ca^{+2}ATPase. *Methods Enzymol.* 157:206–219.

Fujimori, T., and W. Jencks. 1990. Lanthanum inhibits steady-state turnover of the sarcoplasmic reticulum calcium ATPase by replacing magnesium as the catalytic ion. *J. Biol. Chem.* 265:16262–16270.

Girardet, J., Y. Dupont, and J. Lacapere. 1989. Evidence of a calcium-induced structural change in the ATP-binding site of the sarcoplasmic reticulum Ca^{+2}ATPase using terbium formycin triphosphate as an analogue of Mg-ATP. *Eur. J. Biochem.* 184:131–140.

Gruner, S. M. 1981. Controlled humidity gas circulators. *Rev. Sci. Instr.* 52:134–136.

Hanel, A., and W. Jencks. 1990. Phosphorylation of the calcium transporting adenosinetriphosphatase by lanthanum ATP: rapid phosphoryl transfer following a rate-limiting conformational change. *Biochemistry.* 29: 5210–5220.

Herbette, L., P. DeFoor, S. Fleischer, D. Pascolini, A. Scarpa, and J. K. Blasie. 1985. The separate profile structures of the functional calcium pump protein and the phospholipid bilayer within isolated sarcoplasmic reticulum membranes determined by x-ray and neutron diffraction. *Biochim. Biophys. Acta.* 817:103–122.

Herbette, L., J. Marquardt, and J. K. Blasie. 1977. A direct analysis of lamellar x-ray diffraction from hydrated oriented multilayers of fully functional sarcoplasmic reticulum. *Biophys. J.* 20:245–272.

Inesi, G. 1985. Mechanism of calcium transport. *Annu. Rev. Physiol.* 47: 573–601.

Inesi, G., M. Kurzmack, and D. Lewis. 1988. Kinetic and equilibrium characterization of an energy-transducing enzyme and its partial reactions. *Methods Enzymol.* 157:154–189.

Lentz, B., K. Clubb, D. Alford, M. Hochli, and G. Meissner. 1985. Phase behavior of membranes reconstituted from dipentadecanoyl-phosphatidylcholine and the Mg^{+2}-dependent, Ca^{+2}-stimulated adenosinetriphosphatase of sarcoplasmic reticulum: evidence for a lipid domain surrounding protein. *Biochemistry.* 24:433–442.

Lowry, O., N. Rosenbrough, A. Farr, and R. J. Randall. 1951. Protein measurement with folin reagent. *J. Biol. Chem.* 193:263–275.

MacFarland, B., and G. Inesi. 1971. Solubilization of sarcoplasmic reticulum with Triton X-100. *Arch. Biochem. Biophys.* 145:456–464.

MacLennan, D. 1970. Purification and properties of an adenosine triphosphatase from sarcoplasmic reticulum. *J. Biol. Chem.* 245:4508–4518.

Makinose, M. 1969. The phosphorylation of the membrane protein of the sarcoplasmic reticulum vesicles during active calcium transport. *Eur. J. Biochem.* 10:74–82.

Meisner, G., G. Conner, and S. Fleischer. 1973. Isolation of sarcoplasmic reticulum by zonal centrifugation and purification of Ca^{+2} pump and Ca^{+2} binding proteins. *Biochim. Biophys. Acta.* 298:246–269.

Mendelsohn, R., G. Anderle, M. Jaworsky, H. Mantsch, and R. Dluhy. 1984. Fourier transform infrared spectroscopic studies of lipid-protein interaction in native and reconstituted sarcoplasmic reticulum. *Biochim. Biophys. Acta.* 775:215–224.

Moore, B., B. Lentz, M. Hochli, and G. Meissner. 1981. Effect of lipid membrane structure on the adenosine 5′-triphosphate hydrolyzing activity of the calcium-stimulated adenosinetriphosphatase of sarcoplasmic reticulum. *Biochemistry.* 20:6810–6817.

Morrison, J., and W. Cleland. 1983. Lanthanide-adenosine 5′-triphosphate complexes: determination of their dissociation constants and mechanism of action as inhibitors of yeast hexokinase. *Biochemistry.* 22: 5507–5513.

Pascolini, D., and J. K. Blasie. 1988. Moderate resolution profile structure of the sarcoplasmic reticulum membrane under "low" temperature conditions for the transient trapping of E_1~P. *Biophys. J.* 54:669–678.

Pascolini, D., L. Herbette, V. Skita, F. J. Asturias, A. Scarpa, and J. K. Blasie. 1988. Changes in the sarcoplasmic reticulum membrane profile induced by enzyme phosphorylation to E_1~P at 16 Å resolution via time-resolved x-ray diffraction. *Biophys. J.* 54:679–688.

Schwartz, S., J. Cain, E. Dratz, and J. K. Blasie. 1975. An analysis of lamellar x-ray diffraction from disordered membrane multilayers with application to data from retinal rod outer segments. *Biophys. J.* 15:1201–1233.

Shigekawa, M., S. Wakabayashi, and H. Nakamura. 1983. Reaction mechanism of Ca^{2+}-dependent adenosine triphosphatase of sarcoplasmic reticulum. *J. Biol. Chem.* 258:8698–8707.

Shigekawa, M., S. Wakabayashi, and H. Nakamura. 1983. Effect of divalent cation bound to the ATPase of sarcoplasmic reticulum. *J. Biol. Chem.* 253:14157–14161.

Squier, T., D. Bigelow, F. J. Fernandez-Belda, L. deMeis, and G. Inesi. 1990. Calcium and lanthanide binding in the sarcoplasmic reticulum ATPase. *J. Biol. Chem.* 265:13713–13720.

Squier, T., D. Bigelow, and D. Thomas. 1988. Lipid fluidity directly modulates the overall protein rotational mobility of the Ca^{2+}ATPase in sarcoplasmic reticulum. *J. Biol. Chem.* 263:9178–9186.

Stokes, D. L., and N. M. Green. 1990a. Three-dimensional crystals of CaATPase from sarcoplasmic reticulum. Symmetry and molecular packing. *Biophys. J.* 57:1–14.

Stokes, D. L., and N. M. Green. 1990b. A comparison of frozen-hydrated and negatively stained crystals of calcium ATPase suggest a shape for the intramembranous domain. *Biochem. Soc. Trans.* 18:841–843.

Stroud, R. M., and D. A. Agard. 1979. Structure determination of asymmetric membrane profiles using an iterative Fourier method. *Biophys. J.* 25:495–512.

Yamada, S., J. Fujii, and H. Katayama. 1986. Sarcoplasmic reticulum Ca-ATPase: distinction of phosphoenzymes formed from MgATP and CaATP as substrates and interconversion of the phosphoenzymes by Mg^{+2} and Ca^{+2}. *J. Biochem.* 100:1329–1342.